

UNIVERSITÀ DEGLI STUDI DI TORINO

SCUOLA DI SCIENZE DELLA NATURA

Corso di Laurea Magistrale in Fisica



Tesi di Laurea Magistrale

**TEST OF THE BEAM EFFECT ON  
VACUUM ARC OCCURRENCE IN A  
HIGH-GRADIENT ACCELERATING  
STRUCTURE FOR THE CLIC  
PROJECT**

Relatore:

Prof. Martino Gagliardi

Co-relatore:

Dr. Frank Tecker (CERN)

Candidato:

Eugenio Senes

Controrelatore:

Prof. Ferruccio Balestra

Anno Accademico 2015/2016

Considerate la vostra semenza:  
fatti non foste a viver come bruti,  
ma per seguir virtute e canoscenza

Dante, *La Divina Commedia*  
Canto XXVI

# Abstract

*(Leave this for the moment ....)*

A new generation of colliders capable of reaching TeV energies is under development nowadays, and to succeed in this task is necessary to show that the technology for such machine is available. The CLIC project is one of the most advanced design among the possible lepton colliders, and is formed by two normal conducting LINACs. To reach such high energies are necessary accelerating structures carrying gradient beyond 100MV/m and one of the biggest limitations is developing accelerating structures that present a sufficient low occurrence of vacuum arcs. This is pursued both with the design and the *conditioning*, which is the process of increasing the resilience to vacuum arcs of a structure using repetitive RF pulsing sessions.

The focus of this work is on the breakdown rate testing of the TD26 type cavity with and without beam presence inside. At CERN this test has been carried out on the cavity installed in the *dogleg* line in the CLIC-test-facility 3 (CTF3), and connected on the RF side to the X-band test stand 1 (Xbox1).

Other peculiar properties of the operation have been studied also, such has beam-induced RF generation into the cavity after the breakdowns, breakdown migration, ....

# Italian abstract

*(Translate once you have the ok to the english one)*

# Contents

<b>1</b>	<b>Introduction</b>	<b>1</b>
1.1	Generalities on colliders . . . . .	2
1.2	The CLIC project and the CTF3 facility . . . . .	4
1.2.1	Physics and staging . . . . .	4
1.2.2	Main parameters and main issues . . . . .	5
1.2.3	CTF3 . . . . .	8
<b>2</b>	<b>Accelerating structures</b>	<b>9</b>
2.1	Travelling wave accelerating structures . . . . .	9
2.1.1	Reminder of Electromagnetism . . . . .	10
2.1.2	Periodic accelerating structures . . . . .	11
2.1.3	Synchronous particle acceleration . . . . .	13
2.1.4	Figure of merit for accelerating structures . . . . .	13
2.2	High power limits and scaling laws . . . . .	14
2.2.1	Field emission law . . . . .	14
2.2.2	High power limits . . . . .	16
2.2.3	Power flow based criteria . . . . .	17
2.2.4	The modified Poynting vector $S_c$ . . . . .	17
2.3	The TD26CC structure for the Main Beam of CLIC . . . . .	19
<b>3</b>	<b>The breakdown process</b>	<b>22</b>
3.1	Detected effects of breakdowns in accelerating cavities . . . . .	22
3.2	Vacuum arc process description . . . . .	23
3.2.1	Triggers . . . . .	24
3.2.2	Plasma initiation . . . . .	24
3.2.3	Plasma evolution . . . . .	24
3.2.4	Cratering phase . . . . .	25
3.3	Influence of the conditioning process . . . . .	25
<b>4</b>	<b>Experimental setup</b>	<b>27</b>
4.1	Linac and dogleg . . . . .	27
4.1.1	The test setup . . . . .	27
4.1.2	Comparison of setup and CLIC design . . . . .	32
4.2	RF power generation . . . . .	32
4.2.1	The X-Box1 at CERN . . . . .	32
4.3	DAQ & RF control systems . . . . .	34

## CONTENTS

---

4.3.1	Hardware . . . . .	34
4.3.2	Online triggers . . . . .	35
4.4	Other systems . . . . .	35
4.5	Operation of the setup . . . . .	35
<b>5</b>	<b>Data analysis tools</b>	<b>36</b>
5.1	Offline selection of the events . . . . .	36
5.2	Time and space positioning of the breakdowns . . . . .	36
5.3	Migration of the breakdowns . . . . .	36
5.4	Beam induced RF . . . . .	36
<b>6</b>	<b>Results and future developments</b>	<b>37</b>
6.1	Results . . . . .	37
6.2	Further developments . . . . .	37
6.3	Conclusions . . . . .	37
	<b>List of Abbreviations</b>	<b>38</b>
	<b>List of Figures</b>	<b>39</b>
	<b>List of Tables</b>	<b>41</b>
	<b>Bibliography</b>	<b>42</b>

# Chapter 1

## Introduction

Particle accelerators occupy a key role both in fundamental research and in all the applications and industrial processes that uses technology and processes developed initially for the elementary research.

In the fundamental research, accelerators are central to inquire the world at the elementary particle scale. But also the contribution given to the other sciences don't have to be forgotten. In fact a number of examples could be named among the spin-offs of accelerator science, the most notable nowadays is the enormous progress of nanosciences in the last decade. That was made possible by the availability of high-brilliance light sources provided by synchrotrons, that was achievable thanks to the experience developed in the production of high quality electron beams. In the same way inquire a much smaller scale requires machines involving higher energies. Hence in this perspective keep developing the accelerators for the physical research is a fundamental requirement to assure that the cutting-edge technology of today turns into the "labware" of tomorrow for all the other sciences and industry.

Going back to the particle scale, at the moment the most successful model to explain the behaviour of the elementary particles is the *Standard Model*, but it is not conclusive and not able to answer all the questions still open in particle physics. A milestone in favour of the Standard Model was the observation of the Higgs Boson in 2012 [1, 2], and was made possible by the construction of the *Large Hadron Collider* at CERN[3]. However the full understanding of the physics at the particle scale still needs to be achieved. Partially this will be realised with the continued data taking of the LHC, but also the International Committee for Future Accelerators (ICFA) considers that the results of LHC need to be complemented by the results of a lepton collider in the TeV-range[4].

The reason for this is that according to the standard model the hadrons are particles composed of quarks, that are continuously interacting exchanging gluons. This particularity causes the collisions at high energy to be between partons. In addition, there is no way *a priori* to know the energy of the partons involved, so it is impossible to know which will be the energy of the collision. For example it is improbable for a parton in the 14 TeV centre-of-mass energy LHC to have much more than 1-2 TeV of energy at the interaction point[5].

On the other hand, the leptons are pointlike particles, so the interaction is directly involving the two bullets themselves at a given energy, and the number of possible processes that can take place is definitely smaller.

This key difference in the behaviour of leptons and hadrons makes hadron colliders *machines for discovery*, because involve all the possible processes that can take place in a wide range of energies, and the lepton machines *machines for precision*, because the reduced number of possible processes makes the observation of the events of interest much easier.

## 1.1 Generalities on colliders

According to the beam setup two kinds of accelerators can be distinguished:

1. Fixed target: where a beam is shot against a non-moving target. The energy in the centre-of-mass is  $E_{CM} \propto \sqrt{E_{BEAM}}$
2. Colliders: where two beams are accelerated in opposite directions and then made collide with each other. In the case of equal beam energy, in the centre-of-mass  $E_{CM} = 2E_{BEAM}$

Therefore it is easy to see that the collider topology is preferable to reach a high centre-of-mass energy .

In the collisions, the rate of observation of a particular interaction process A is given by

$$\frac{dN(A)}{dt} = \mathcal{L} \sigma(A) \quad (1.1)$$

where  $\sigma$  is the process cross-section, which depends by the physics of the process A itself, and  $\mathcal{L}$  is the luminosity, which depends entirely on the accelerator. Therefore the figure of merit when it comes to talk about accelerators is the luminosity, which is given by

$$\mathcal{L} = H_d \frac{N^2}{\sigma_x \sigma_y} n_b f_r \quad (1.2)$$

where  $N$  is the number of particles per bunch,  $\sigma_x$  and  $\sigma_y$  are the beam dimensions in the horizontal and vertical plane,  $n_b$  is the number of particle per bunch,  $f_r$  is the collision frequency of the bunches and  $H_d$  is a correction factor that takes in account the non-ideality of the collision, such as crossing angle, collision offset, hour glass effect, non gaussian beam profile and so on.

It is necessary to reach the highest luminosity possible since the events that are going to be studied are rare. This is realised differently according to the design of the accelerator in use:

- linear accelerators (linacs): have a low repetition frequency, typically lower than hundreds of Hz and the beam is passing just once to be accelerated through the machine.

- circular accelerators (typically synchrotrons): have a higher repetition frequency, up to tenth of kHz, and are keeping the particle beam in orbit for many turns, so can accelerate it over a long period of time

After this distinction one could be led to think that the circular machine is the best choice in any case in order to reach high luminosity, but raising the energy of the beam becomes problematic: in fact the power loss in circular machines due to the emission of synchrotron radiation scales according to the following expression

$$P \propto \frac{1}{\rho^2} \frac{E^4}{m_0^4} \quad (1.3)$$

where  $\rho$  is the bending radius of the machine,  $E$  is the particle energy and  $m_0$  is its rest mass. As can be noted in the table 1.1, the energy loss per turn is a relevant fraction of the beam energy, e.g. for the LEP machine more than 3 GeV were lost per turn, at the highest energy per beam of 104.5 GeV. To raise the beam energy and reduce the energy loss, the radius of circular machines escalates quickly. Simply scaling LEP, it is possible to show that in order to reach the centre-of-mass energy of 3 TeV, the circumference should be increased to thousands of kilometers [6]. To solve the issue, the development of new lepton colliders is focusing on two different solutions:

1. Use muons instead of electrons: this innovative approach reduces the power lost because of the higher mass of the muon compared to the electron, but has to deal with the short life of muons, which is roughly  $2 \mu s$  in the rest frame
2. Limit the losses caused by synchrotron radiation, either by increasing the bending radius or abandoning the circular topology for the linear one

It has to be noted that the muon technology is rather new and still needs to be fully developed, while the linear accelerator technology profits of the progress achieved in the last half century mainly in CERN, SLAC and KEK.

In this perspective a number of project are under study at the moment, of which the most ambitious are FCC-ee, *Future Circular Collider*, ILC, *International Linear Collider*, and CLIC, *Compact Linear Collider*. The first one consist of a circular collider which is supposed to be placed in a 80-100 km long tunnel before the installation of the FCC-hh, the others are linacs even if based on completely different technologies and solutions. A comparison of the features of these projects in the final stage is presented in table 1.1, together with LEP as an example of a circular lepton collider.

Furthermore a recent interest arose in more compact technologies, e.g. plasma acceleration techniques, but the reliability of such designs still needs to be proven in the perspective of creating a fully functional machine that goes beyond the demonstration of the working physical principle.

Parameter	LEP2	FCC-ee	CLIC		ILC
$\sqrt{s}$ [GeV]	209	350	500	3000	500
$\mathcal{L}_{peak}$ [ $10^{34} \text{ cm}^{-2} \text{ s}^{-1}$ ]	0.012	1.3	2.3	5.9	1.8
Total lenght [km]	26.7	100	13	48.4	31
$E_{acc}^{loaded}$ [MV/m]	5 - 9	10 - 20	80	100	31.5
Bunch population [ $10^9$ ]	105	170	6.8	3.72	500
Bunch spacing [ns]		4000	0.5	0.5	554
Collision rate [Hz]		$\approx 3000$	50	50	5
$\epsilon_x^* / \epsilon_y^*$ [ $\mu\text{m}/\text{nm}$ ]		0.68/0.68	2.4/25	0.66/20	10/35
$\sigma_x^* / \sigma_y^*$ [nm]		3600/70	202/2.3	40/1	474/5.9
Energy loss [GeV turn $^{-1}$ ]	3.34	7.55	-	-	-
AC Power [MW]	120	$\approx 300$	271	582	163

Table 1.1: Comparison of two circular machines, LEP[7, 8] and FCC-ee[9, 10] and the two projects for linear machines, the fist and last stage of the CLIC implementation [11] and the ILC[12]

## 1.2 The CLIC project and the CTF3 facility

The *Compact Linear Collider* is the project for a linear electron-positron collider capable of reaching a centre-of-mass collision energy of 3 TeV and a luminosity of  $2 \times 10^{34} \text{ cm}^{-2} \text{ s}^{-1}$  in the final stage.

### 1.2.1 Physics and staging

The machine is designed to be built in 3 stages, with a final energy of 3 TeV.

Since the Conceptual Design Report (CDR)[11] was released just before the discovery of the Higgs boson, the centre of mass energy stages have been reshaped in order to be able to access interesting measurements. For a given centre-of-mass energy stage, the energy can be modified by a third with limited loss of performance[13], allowing an eventual retuning of the energy of the stages following the results of the LHC physics campaign.

The energy staging has been chosen with the idea to access the Higgs and top physics from the first stage.[14, 15]

In the first stage at 380 GeV the measurements on the Higgs physics can be conducted through Higgsstrahlung and WW-fusion processes, thereby providing accurate model-independent measurements of Higgs couplings to bosons and fermions[16]; the top physics measurements will be focused on the  $t\bar{t}$  pair production threshold in the vicinity of  $\sqrt{s} = 350$  GeV.

The second stage is proposed at 1.5 TeV and allows to access new physics phenomena and additional properties of the Higgs boson and the top quark, such as Higgs self-coupling and rare Higgs branching ratios.

The third stage is proposed at 3 TeV and will give direct access to pair-produced particles with mass up to 1.5 TeV or single particles with mass up

to 3 TeV. This stage is particularly interesting as test for the Beyond Standard Model theories, since such high energy in a lepton machine makes the observation of new particles much easier than in the LHC.

A further adaptation of these steps is possible after the publication of the results of the run 2 of the LHC, in any case the advantage of a linear machine in this sense is that the final energy can be reshaped modifying the total length of the machine. In figure 1.1 is shown the footprint of a possible CLIC built in the Geneva area, in order to give an idea about the order of magnitude of that kind of facility compared to LHC.



Figure 1.1: Map of the CLIC facility, if implemented in the Geneva area

### 1.2.2 Main parameters and main issues

The realisation of such machine implies many technological challenges in order to keep the power consumption and the dimension limited while matching the design goal parameters. These challenges have been faced developing the novel *two-beam acceleration scheme*, in which the idea is to use a high-current and low-energy beam, the *Drive Beam*, in order to generate the RF power to accelerate a low-current and high-energy beam used for the experiments, named *Main Beam*.

The Drive Beam is produced using a dedicated linac, and then the current is multiplied using a delay loop and two recombination rings, reaching a combination factor of  $2 \times 3 \times 4 = 24$ . This topology generates the beam with a final frequency of the bunches of 12 GHz. It is essential to reach the highest possible efficiency in the Drive Beam production, in order to shrink the power

## CHAPTER 1. INTRODUCTION

---

consumption to the smallest possible. To reach this goal the acceleration in the linac is performed using the accelerating cavities in fully-loaded mode.[17]

While the biggest challenge for the Drive Beam is reaching the necessary high current, for the Main Beam the hardest challenge is generating a beam with the smallest dimension possible, in order to increase the luminosity of the machine as much as possible.

The Main Beam is produced in a separate facility, where a DC-photo gun system provides the initial polarised electron beam. Afterwards part of the beam is sent to a target in order to generate the positron beam. Once both beams have been produced, they are sent to the next accelerating stages, which are composed of linacs to raise the beam's energy and of damping rings to reduce the emittances.

The detailed description of the Main Beam production and the Drive Beam recombination process can be found in [11]. The working principle have been demonstrated in the CTF3 [18].

Both beams are sent to the common tunnel where the Two-beam modules are installed. The Two-beam module is composed of two principal sections, which are the PETS, *Power Extraction and Transfer Structures*, and the accelerating structures for the Main Beam, as shown in figure 1.3. The Main Beam passes through the PETS and gets decelerated. As product of the deceleration a pulse of RF power is produced, which is transferred by a waveguide network and used to accelerate the Main Beam.

In this way it is possible to reach an efficient acceleration of the Main Beam up to the desired energy for the experiments.

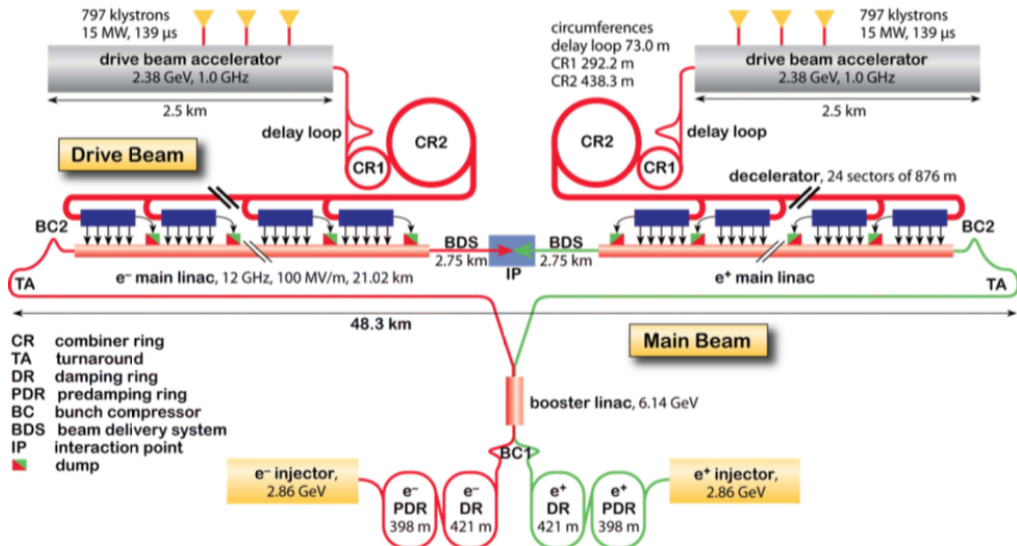


Figure 1.2: Layout of the final stage of CLIC

There are many issues that can affect the performance of a machine like CLIC, and need to be analysed carefully since no similar machine has been built so far.

## CHAPTER 1. INTRODUCTION

---



Figure 1.3: Design of a Two-beam module.

The main issues are:

1. 100 MV/m accelerating gradient: this requirement comes from the final energy of 3 TeV and the requirement of a maximum length of 50 km
2. Breakdown rate  $< 3 \times 10^{-7}$  breakdowns per pulse per meter: this limitation comes from the limit on design luminosity loss in case of breakdown. Is the aim of this work and will be stressed in detail later
3. Transverse wakefields limitation: wakefields have to be considered because of the short bunch spacing in the bunch train. If not limited are a serious issue to the luminosity.
4. Powering the accelerating structures: the klystrons on the market are not able to produce a high-power RF pulse 150-200 ns long with a high efficiency. Sacrificing the request of high efficiency, it is possible to use klystrons equipped with pulse compression systems. This option is not practicable for a long accelerator because of the excessive power consumption, but is kept in consideration in case of a reduction of the length.
5. Generate the drive beam with an efficiency of 97% in order to contain the power consumption. Also the efficiency of the power transfer between the beams is a key issue in order to reach the energy goal

6. Extremely small beam emittance and size: in order to match the luminosity goal with the typical low repetition rate of a linac it is necessary to squeeze the beam as much as possible, reaching the goal of 40 and 1 nm at the interaction point in the horizontal and vertical plane. This parameter includes the realisation of a nanometric alignment and vibration stabilisation system

Therefore the parameters in table 1.2 have been selected in order to match the design parameters reported in table 1.1 for the top design energy.

Description	CLIC 3 TeV
Peak luminosity [cm <sup>-2</sup> s <sup>-1</sup> ]	2.0x10 <sup>34</sup>
Total site length [km]	48.4
Loaded accelerating gradient [MV/m]	100
Main LINAC RF frequency [GHz]	12
Charge per bunch [nC]	3.7x10 <sup>9</sup>
Bunch separation [ns]	0.5
Bunches per train	312
Beam pulse duration [ns]	156
$\epsilon_x^* / \epsilon_y^*$ [ $\mu\text{m}$ ]/[nm]	0.66/20
$\sigma_x^* / \sigma_y^*$ [nm]	40/1

Table 1.2: CLIC main parameters in the final stage

### 1.2.3 The CLIC Test Facility 3

To be able to affirm that the CLIC scheme is a feasible and a reliable technology to build a functional collider, a number of tests have to be conducted since no accelerators using the Two-beam acceleration concept have been built. The CLIC Test Facility 3 have been built and operated at CERN in order to demonstrate experimentally:

- The feasibility of the Drive Beam generation with a frequency of 12 GHz, performing the beam recombination using a delay loop and a combiner ring for a total multiplication factor of  $2 \times 4 = 8$
- The RF power production using the PETS and investigate possible issues of the Two-beam scheme

In addition a branch of the linac was used to perform high-gradient tests with the beam presence inside the accelerating cavity, which is the topic of the following work. A more detailed description will follow in chapter 4.

# Chapter 2

## Accelerating structures

The accelerating structures are one of the key parts of a particle accelerator. Even though in the first accelerators the particle acceleration was achieved simply with fixed fields, this technique showed its limitations quite soon due to the impossibility to create arbitrary high DC voltages without being subjected to electrostatic discharges. The present conventional technology for particle acceleration is based on RF cavities, so it is natural try to push the state-of-the-art technology the furthest possible in order to reach the highest acceleration possible in the shortest length. In the case of the CLIC project a key issue is to be able to produce cavities with an accelerating gradient of 100 MV/m, which is the cutting-edge value at the moment when keeping the breakdown rate limited.

In this chapter some topics about the theory of accelerating cavities will be presented. The aim is to give to the reader a theoretical introduction to be able to understand the description of the cavity under test.

### 2.1 Travelling wave accelerating structures

In this section some useful concepts and result of the electromagnetic theory will be recalled. Because of conciseness, the examples and the geometries presented will refer to travelling wave accelerating structures, since it is the only type of structure used in this work. The curious reader can find details on the untreated topics in [19, 20, 21] and in plenty of specialised books.

### 2.1.1 Reminder of Electromagnetism

#### Maxwell's equations

It's well known since the basic courses of physics that the propagation of the electromagnetic fields follow the Maxwell's equations, that in a medium are

$$\begin{aligned}\nabla \cdot \vec{D} &= \rho_{free} \\ \nabla \cdot \vec{B} &= 0 \\ \nabla \times \vec{E} &= -\frac{\partial \vec{B}}{\partial t} \\ \nabla \times \vec{H} &= \vec{J}_{cond} + \frac{\partial \vec{D}}{\partial t}\end{aligned}\tag{2.1}$$

where  $\vec{E}$  and  $\vec{B}$  are the electric and magnetic field in the vacuum,  $\vec{D} = \epsilon \vec{E}$ ,  $\vec{B} = \mu \vec{H}$  and  $\vec{E} = \sigma \vec{J}$ . The propagation in vacuum is described by the same equations and can be easily derived with an appropriate choice of the constants.

#### Waveguides and resonant cavities

In some particular cases the confined propagation of electromagnetic waves is possible, and is commonly realised using a metal waveguide to direct all the energy in a single direction. In this section some useful results on the propagation in a waveguide will be stressed, the full derivation can be found in literature [22, 23, 19].

The request of propagation in the direction of the axis of the waveguide can be traduced to the condition  $\vec{E} \times \vec{n} = 0$ , that means asking that no power is dissipated in the walls of the cavity by Joule effect since the electric field is normal to the surface anywhere and anytime.

Many solutions can be found to the problem, integrating the Maxwell's equations with the given boundary condition, but without entering in the calculations, the interesting solutions belong to two classes:

- **TM modes:** Transverse Magnetic modes, where the axial component of the magnetic field is null
- **TE modes:** Transverse Electric modes, where the axial component of the electric field is null

Every mode has a particular cutoff frequency, and will propagate only in case that the condition  $\omega > \omega_c$  is met (where  $\omega_c = 2\pi f_c$  and  $f_c$  is the cutoff frequency of the mode). The cutoff frequency of each mode depends mainly on the geometry of the guide utilised, and waves with a frequency lower than the cutoff frequency will be exponentially damped.

The major features of a waveguide are: the *phase velocity* is  $v_p = \frac{\omega}{k} > c$ ; the *group velocity* instead is  $v_g = \frac{\partial \omega}{\partial k} < c$  as expected for the physical quantity representing the speed of propagation of the EM wave according to Relativity; and the dispersion relation for a uniform waveguide can be expressed as

$$\omega^2 = \omega_c^2 + (k_0 c)^2\tag{2.2}$$

where  $\omega_c = K c$  and  $K$  is the cutoff wavenumber.

The waveguides are a key building block of particle accelerators to deliver the RF power from the production equipment to the accelerating cavities, but are not suitable for particle acceleration as pointed out later.

A particular case is represented by *Resonant Cavities*, which are in the simplest case closed waveguides at the terminations (e.g. a cylindrical cavity, or *pillbox cavity*, is composed of a circular waveguide closed by two planes at the extremities). In resonant cavities the EM field can resonate according to the particular eigenfrequencies of the system, which are mainly dictated by the geometry. This process allows propagation of just a set of frequencies, just like in the WGs, but when a cavity is operating at one of the eigenfrequency starts to accumulate energy because of the resonance. This mechanism is utilised in accelerating structures.

### 2.1.2 Periodic accelerating structures

To reduce the phase velocity into the structure, it is possible to load it with additional metallic walls placed orthogonally to the axis of the cavity. Such structures are named *Disk (or Iris) Loaded Accelerating Structures*. A schematic example is presented in figure 2.1



Figure 2.1: Scheme of a travelling wave, disk loaded accelerating structure. The drawings illustrates the input and output couplers, the disks loading the cavity and the beam passing through the irises. From [24]

The accelerating structure is composed of *cells*, which are connected by the *iris* to the adjacent cells. At the beginning and the end of the structure two special cells form the input and output coupler for the RF. The role of the irises is creating a free path for the passage of the beam and allowing the propagation of the EM field from the input coupler to the output one. In the case of room temperature cavities the material normally used is Copper, while for superconducting cavities the material can vary and also metallic cavities coated internally with a superconductive layer are a possibility.

From the field perspective, the fact that the accelerating structure is loaded with the disks changes the way that the EM waves propagate in the structure. The full mathematical description, is found in [23, 19], here simply a general idea of the process and of the relevant results is given.

The geometry of the accelerating structure can be seen as a cylindrical cavity loaded regularly with the disks. If as first approximation we consider an infinite structure, it is possible to use the *Floquet's Theorem*, that can be summarised as follows: "*In a given mode of an infinite periodic structure, the fields at two different cross sections that are separated by one period differ only by a constant factor, which in general is a complex number*". This has two main implications: there are some regions of the spectrum of  $\omega$  that don't allow the waves to propagate, called *stopbands*, and others, called *passbands*, where the propagation is allowed with a *phase shift*  $\Delta\phi = k_0 d$ , where  $d$  is the length of the cell. The phase advance per cell is a particular parameter of every structure, and is defined in the design phase.

The waves that are allowed to propagate in such conditions are called *Space Harmonics*, and can be seen as an infinite number of waves propagating at the same frequency but with different wavenumbers. The dispersion relation becomes

$$\omega^2 = \omega_c^2 + c^2 \left( k_0 + \frac{2\pi n}{d} \right)^2 \quad (2.3)$$

where the principal wave of the mode has  $n = 0$  and the others have  $n$  according to the direction of propagation.

The phase velocity of the  $n$ -th harmonic becomes

$$\beta_n = \frac{\omega}{k_n c} = \frac{\beta_0}{1 + n\beta_0 \lambda/d} \quad (2.4)$$

which allows to reach an arbitrary low phase velocity, as requested for the particle acceleration.

The comparison of the phase velocity of a waveguide and accelerating structure is presented in figure 2.2.



Figure 2.2: Brillouin diagram of a uniform waveguide (red) compared to a disk-loaded accelerating structure (green) [25]

### 2.1.3 Synchronous particle acceleration

A particle injected in an electromagnetic field in some conditions can gain energy at expense of the field, getting accelerated. This is realised in travelling-wave structures injecting the particle at the right moment and ensuring that the field and the particle have a similar speed. In this manner the particle can travel with the field with an energy gain given by

$$\Delta W = qV_0 \cos\phi \quad (2.5)$$

where  $q$  is the charge of the particle,  $V_0$  is the accelerating field and  $\phi$  is the relative phase between particle and RF field.

In order to deliver a constant energy gain to a charged particle it is necessary to shape the EM field matching two fundamental conditions:

1. The electromagnetic wave has to have a non-zero component in the direction of the motion of the particle
2. The phase velocity of a wave has to be similar to the particle velocity

using some results of the theory of EM waves it is possible to show that the two condition cannot be met neither in the free space, nor in simple waveguides, but is necessary to build up some particular structures in order to coerce the electromagnetic field to propagate in the desired form.

### 2.1.4 Figure of merit for accelerating structures

To characterize different accelerating structures, is necessary to rely on some significant quantities that can be derived from the geometry of the cavities. The most important figures of merit (FOMs) are the following (a number of different definitions are commonly used, here are reported in accordance with [26]):

- **Quality factor**

$$Q_0 = \frac{\omega_0 U}{P_{loss}} \quad (2.6)$$

is a standard FOM for the resonant cavities, representing the stored energy  $U$  over the power dissipated  $P_{loss}$

- **Shunt impedance**

$$R = \frac{V_{acc}^2}{2P_{loss}} \quad [M\Omega] \quad (2.7)$$

represent the effectiveness of producing an axial voltage  $V_{acc}$  for a given power dissipated. For long cavities, where it is preferable to have a quantity that is independent from the length of the structure, the Shunt impedance per unit length  $Z$  is commonly used

$$Z = \frac{R}{L} \quad [M\Omega/m] \quad (2.8)$$

where  $L$  is the length of the cavity.

- **R over Q**

$$\frac{R}{Q} = \frac{(V_{acc})^2}{2\omega_0 U} \quad [M\Omega] \quad (2.9)$$

represents the relation between the accelerating field  $V_{acc}$  and the stored energy  $U$

- **Filling time (for travelling-wave structures)**

$$t_F = \int_0^L \frac{dz}{v_g(z)} \quad (2.10)$$

is time needed by the EM field to fill the structure

- **Power delivered to the beam**

$$P_B = \frac{I \Delta W}{q} \quad (2.11)$$

where  $I$  is the beam current and  $\Delta W$  is the energy gain

- **Beam loading ratio**

$$\epsilon_s = \frac{P_B}{P_{tot}} \quad (2.12)$$

represents the fraction of power that is delivered to the beam

## 2.2 High power limits and scaling laws

The limiting factors for room-temperature high-gradient accelerators have been identified as *field emission* and *RF breakdown*. The former is the emission of electrons in the form of the so called "*Dark current*", that subtracts RF power, causes radiation and can produce wakefields; the latter is a limiting factor to the operation of accelerators and can damage the structures.[27]

The understanding of these phenomena is particularly challenging and requires a mixture of notions of disciplines such as surface physics, metallurgy, fabrication processes, microwaves, beam dynamic and plasma physics. At the moment a satisfactory unified theory of the processes that take place during the breakdowns has not been found yet. The improvement of the structures is achieved using scaling laws for the high power limitations, that have been deducted from the experience and the experiments on the structures tested so far.

### 2.2.1 Field emission law

#### Emission from flat clean surface

The field emission law was theorized by Fowler and Nordheim in 1928 and rules the current emission from a metal with an intense electric field applied. The

derivation was carried out calculating the tunneling probability of electrons of the conduction band through the perfectly flat and clean surface of a metal. The applied electric field modifies the potential barrier, and the current density of emitted electrons can be derived as the following, giving the *Fowler-Nordheim equation* [28]

$$J_F = \frac{1.54 \times 10^{-6} \times 10^{4.52\phi^{-0.5}} E^2}{\phi} \exp\left(-\frac{6.53 \times 10^9 \phi^{1.5}}{E}\right) \quad [A m^{-2}] \quad (2.13)$$

where  $\phi$  is the work function of the material and  $E$  is the applied electric field.

### Enhanced field emission

It is well known that almost any surface is never perfectly clean and flat, and also the fact that the asperities of the surface provoke an enhancement of the local electric field. This behaviour lead to the phenomenon known as *Enhanced Field Emission* (EFE), which major contributors are:

- Surface imperfection due to imperfect machining
- Metallic dust
- Molten craters after breakdowns
- Absorbed gas

and some others. These effects can create particular sites known as "emitters". It is a common praxis define the field enhancement factor  $\beta$  to relate the electric field to the microscopic one

$$E_m = \beta E_0 \quad (2.14)$$

The  $\beta$  factors can be calculated according to the emitter's geometry [29] as exploited in figure 2.3. Once the local field is known, using Eq. 2.13 calculate the current emitted from EFE by an emitter site of area  $A$  gives

$$I_F = \frac{1.54 \times 10^{-6} \times 10^{4.52\phi^{-0.5}} A \beta^2 E^2}{\phi} \exp\left(-\frac{6.53 \times 10^9 \phi^{1.5}}{\beta E}\right) \quad [A] \quad (2.15)$$

where  $\beta E$  is the local field,  $\phi$  is the work function of the material and  $A$  the area of the considered emitter.

In the RF case the average current emitted is given by similar calculations, averaging the electric field on an RF period [27].

Experimental evidence of the dark current emission have been detected by setups equipped with Faraday Cups, as in [30].

The emission of dark current seems to be a precursor of the breakdown process, even if the relationship between the two processes has not been clarified so far.



Figure 2.3: Field enhancement factors for simple geometries of metallic protrusions, plotted as function of geometrical features. From [29]

### 2.2.2 High power limits

In an historical perspective, the Kilpatrick's Critereon was the first attempt to create a high power limit for the vacuum breakdown valid both in DC and RF applications [31]. The model was based on the acknowledgement of the Field Emission, and suggesting that the vacuum arc was created by the cascade of secondary electrons ejected from the surface by ion bombardment. The main result was to find a law ruling the maximum electric field achievable without triggering a breakdown.

This critereon was reviewed many times up to now, because the experiments conducted nowadays show a field limit 7-8 times higher than Kilpatrick's prediction. This can be addressed to different reasons: first of all the quality of the machining of the structures has increased considerably since the 1950's; in second instance Kilpatrick examined simple geometries, while in RF cavities are more complicated.

At the end of the 1980's J.D.Wang finally proposed a model based on microprotrusion effect on the field and field emission, that involves the formation of a micro-plasma during the breakdown process. Also the Kilpatrick's limit was revised again in order to match the experimental results. [32, 33]

Furthermore theories on the mechanism of breakdowns evolved, and will be mentioned in chapter 3.

Without entering in the physics of the breakdown phenomenon yet, the two following scaling laws are currently used in the design of modern accelerating structures.

### 2.2.3 Power flow based criteria

Other scalings have been proposed, like the phenomenological  $P/C$ -criterion, where  $P$  is the power flowing in the cavity and  $C$  the minimum iris circumference. It is straightforward to see that this is strongly related to the maximum surface electrical field, which is stronger for smaller irises. It has to be underlined that this is suitable just to travelling wave structures (TWS), since the power flow in standing wave structures (SWS) is close to zero.

In recent years a more advanced version of the scaling has been presented [34], which is quantified by

$$\frac{P\tau^{1/3}}{C} \quad (2.16)$$

where  $P$  is the power flow through the structure,  $\tau$  the pulse length and  $C$  the minimum iris circumference. This has also been formulated as  $(f \times P/C)^{0.5}$ , which is a quantity linear with the field [35].

Anyway, although these criteria are still in use today for the accelerating structure design, finding a more general criterion valid for any type of cavity is necessary.

### 2.2.4 The modified Poynting vector $S_c$

During the development of high-gradient normal conducting accelerating structures for the CLIC project, a new field quantity was developed, the *Modified Poynting Vector*  $S_c$ , that is suitable both for TWS and SWS. [36]

The formulation is based on two assumptions: the breakdown process is determined by the accumulation of the pulses rather than the single pulse and the possible triggers of the breakdown can be induced by many processes that will be discussed later and are not relevant for the scaling law derivation.

A number of effects have to be taken into account (a simple geometry is considered, a cylindrical protrusion surmounted by a hemispherical cap):

#### Pulsed heating by field emission current

it is known that the field emission gets enhanced by the presence of the protrusion as described before. In this case the field enhancement factor can be expressed as  $\beta \simeq h/r$ , where  $h$  is the tip height and  $r$  is the cap radius. So the tip will emit a current according to the Fowler-Nordheim law 2.15, causing in first approximation the heating of the tip due to the ohmic heating as shown in figure 2.4. Assuming that the edge of the tip will be the most heated part, and using the heat conduction equation, it is possible to derive the emitted current to melt the tip, which is found to be approximately  $36 \text{ A}/\mu\text{m}^2$  for a tip of  $1 \mu\text{m}$  height and a pulse of 100 ns. This is consistent with the findings in [37]. The  $\beta$  factor can be then derived, which is approximately between 40 and 60 considering a surface electric field in case of breakdown between 200 and 300 MV/m, according with the experimental results.



Figure 2.4: (a) Electric field distribution around the protrusion considered. (b) Field emitted current and power flow. In both the plots arrows indicate the direction of the field and the color code the absolute value of the field, mapped logarithmically.[36]

### Power flow near an emission site

The heating of the tip mentioned before requires a huge amount of energy, which can be supplied only by the RF power present into the cavity. This is described by the Poynting vector  $S_{RF} = E \times H_{RF}$ . As discussed before a current is established in the tip, and flows through, subtracting energy to the EM field in the surroundings of the tip. The current flows through the tip and leave it at the edge, getting sprayed in the cavity according to the Fowler-Nordheim theory. Since any current flowing creates an associated magnetic field, the power flow due to the emission is given by  $S_{FN} = E \times H_{FN}$ .

The key point is that since the copper is a very good conductor, to provoke a notable ohmic heating of the tip, a significant power flow through the tip is necessary. This can be calculated evaluating the  $S_{FN}$  at a distance  $d = h$  from the edge of the tip, where the electric field is not perturbed anymore by the shape of the tip itself. This can be formulated as the condition

$$P_{RF} \geq P_{FN} \gg P_{loss} \quad (2.17)$$

where  $P_{loss}$  is the power lost for ohmic heating and  $P_{FN}$  the power flow through the tip.

Considering now the relative phase of the  $P_{RF}$  and of the  $P_{FN}$  it is possible to derive an expression for the power emitted from the tip in a copper cavity

$$P_{FN}(t) = A E_0^3 \sin^3 \omega t \exp\left(\frac{-62}{\beta E_0 \sin \omega t}\right) \quad (2.18)$$

where the work function of the copper  $\phi = 4.5 \text{ eV}$  has been used,  $A$  is the area of the conductor and  $\omega = 2\pi f$  is the angular velocity.

The RF power can be divided in real and imaginary part, with a phase shift of  $90^\circ$ . The real part is the energy propagating into the structure only

and the imaginary part is the energy stored in the cavity both magnetically or electrically as it is the case in every resonant cavity. Since the active power flow is more efficient than the reactive one in providing power for the field emission, a weighting factor  $g_c$  is introduced. The values of  $g_c$  are slowly as function of the local electric field. For practical reasons all the simulation codes work using the complex Poynting vector  $\bar{S}$ , the precedent reasoning can be adapted to follow this practice, using the *Modified Poynting Vector*

$$S_c = \text{Re}\{\bar{S}\} + g_c \text{Im}\{\bar{S}\} \quad [\text{W}/\mu\text{m}^2] \quad (2.19)$$

Since this quantity can be calculated in any point of a structure, this allows to identify in advance the regions which are more sensible to the breakdown process. The rule of thumb given by the experience says that this quantity should not exceed the value of  $5 \text{ W}/\mu\text{m}^2$  to have a breakdown rate smaller than  $1 \times 10^{-6} \text{ bpp m}^{-1}$  with a pulse length of 200 ns.

This quantity has been used to design all the latest generations of CLIC structures, including the one tested in this work.

## 2.3 The TD26CC structure for the Main Beam of CLIC

After the precedent part about the general laws that regulate the operation of the TWS, now the structure under test in this work, the TD26CC, will be presented. The name stays for Tapered, Damped, 26-cells active cells structure with Compact Couplers.

It is necessary to keep in mind that in the design of the real cavities, it is almost never possible to use the general laws described in precedence because of the high complexity of the geometry. A great work of design and simulation is necessary, and is carried out with complex numerical simulations. This section will present a summary of the parameters and features of the cavity, the details can be found in [11, 38, 39].

As pointed out in [11], the main constraints in the structures for the main beam linac are

1. Maximum surface electric field:  $E_{surf}^{max} < 260 \text{ MV/m}$
2. Pulsed surface heating:  $\Delta T^{max} < 56 \text{ K}$
3. Power density:  $P_{in}/C\tau_p^{1/3} < 18 \text{ MW/mm ns}^{1/3}$

These limitations, together with the parameters listed in section 1.2.2, lead to the current design after a careful optimisation and tradeoff of the parameters. The main parameters are reported in Table 2.1

The structure is fabricated stacking machined copper disks that are brazed together with a particular procedure that has been elaborated in order to achieve the highest mechanical precision possible in the alignment of the parts. Figure 2.5 shows a disk and a model of the accelerating structure.

Average loaded accelerating gradient	100 MV/m
Frequency	12 GHz
RF phase advance per cell	$2/3\pi$ rad
Average iris radius to wavelength ratio	0.11
Input, output iris radii	3.15, 2.35 mm
Input, output iris thickness	1.67, 1.00 mm
Input, output group velocity	1.65, 0.83 % of c
First, last cell Q-factor	5536, 5738
First, last cell shunt impedance	81, 103 MΩ / m
Number of regular cells	26
Structure length including couplers	230 mm
Filling time	67 ns
Total pulse length	242 ns
Peak input power	61.3 MW
RF-to-beam efficiency	27.7 %
Maximum surface electric field	230 MV/m
Maximum pulsed surface heating	47 K

Table 2.1: Parameters of the structure

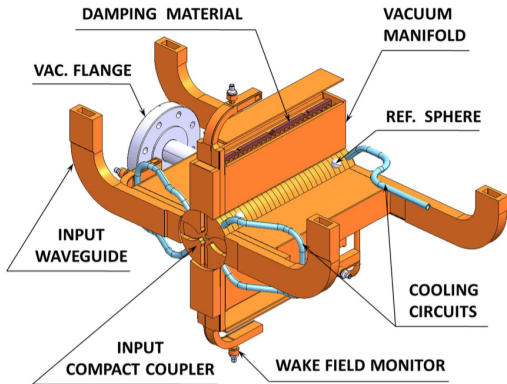
The iris radius and thickness are linearly tapered in order to optimise the various high power parameters and to create a smooth field profile along the structure.

Because of the high number of bunches per train and of the very short spacing between them (see table 1.1), the structure is realised in order to extract the transverse wakefields that can develop in the structure. This is realised using 4 symmetrical waveguides of dimensions carefully selected in order to allow the propagation of just the higher order electromagnetic modes (HOMs) but not the fundamental one that is used to accelerate the bunches and is provided from the input couplers. Once extracted, the transverse wakefields are damped on tips of Silicon Carbide (SiC) that are placed 50 mm away from the axis of the cavity. The tapering also provides detuning of the high order modes, which are an issue even for highly damped structures.

Cooling water circuits and the vacuum flange are also installed the structure. The "CC" in the initials of the cavity name refers in fact to the particular shape of the coupling cells of this structure.



(a) A disk composing the structure



(b) CAD model of the structure, open to show the damping material

Figure 2.5: A disk composing the structure (left) and the scheme of an accelerating structure (right), including couplers for the RF, cooling elements and connection flanges. The wakefield monitor is not present in the prototype under test

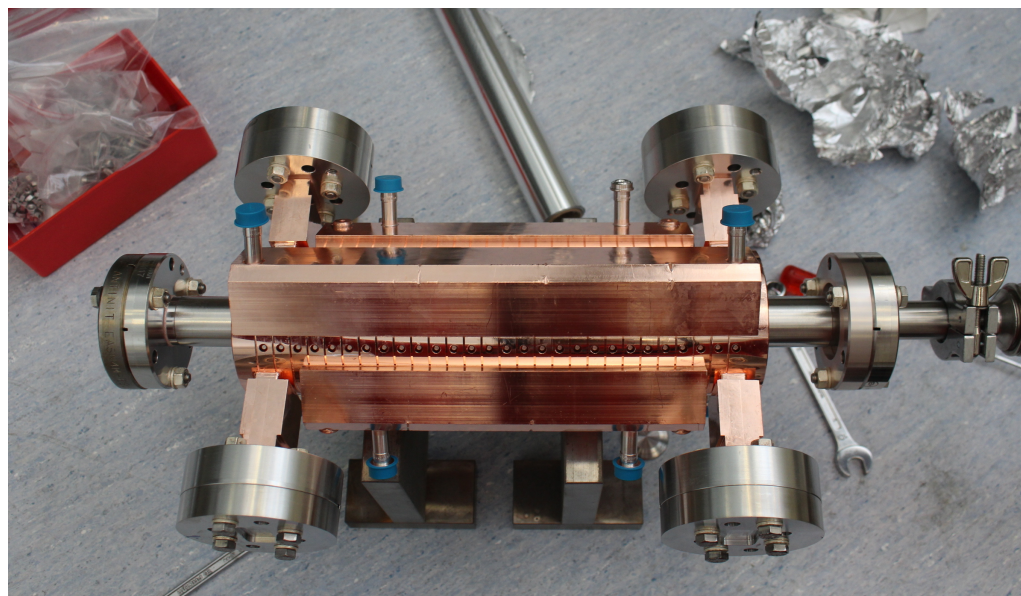


Figure 2.6: The structure prototype before the installation (*Photo A. Solodko*)

# Chapter 3

## The breakdown process

In this chapter the detectable effects of the breakdowns and a possible model will be presented. The setups for studies on the breakdown physics will not be presented instead, and a good review can be found in [25]. The reason is that using the setup object of this work it is just possible to have a glimpse on the beam effect, but not perform the measurements related to the traditional breakdown physics. This is caused by the beam losses, that make the majority of the sensors that are normally used blind.

Researching a model for the breakdowns is particularly complicated, because of the wide variety of experimental conditions where tests are made. Researchers anyway converge on the fact that, at low pressures, the vacuum arc initiation process is dependent by the surface and material properties, but is independent from the pressure itself [40].

Strong efforts in pursuing the understanding of the phenomenon have been made so far, with the result of the improvement of the maximum gradient achievable in accelerating structures and the development of the first simulation codes [41].

### 3.1 Detected effects of breakdowns in accelerating cavities

Most of the theories about breakdown converge on the fact that the breakdown and the field emission are different phenomena. While the field emission is always present, the breakdown of the field is a rare event, and depends by many causes, first of all the material.

Therefore in the detection of the breakdown a background current emitted by FE is always present, but on top of that are appreciable during the breakdown [42]:

- RF pulse reflection: after the breakdown the incoming power is reflected back, causing a fall of the transmitted power and the raise of the reflected power

- X-ray production: an isotropical emission of X-rays is appreciable, but passing through the structure any information carried by the spectrum is lost
- Visible light emitted by the arc
- Current bursts exiting the cavity
- Vacuum level spikes: this effect fades while the conditioning continues. Will be discussed in the section 3.3

Other effects, such as shock waves, have also been appreciated [43].

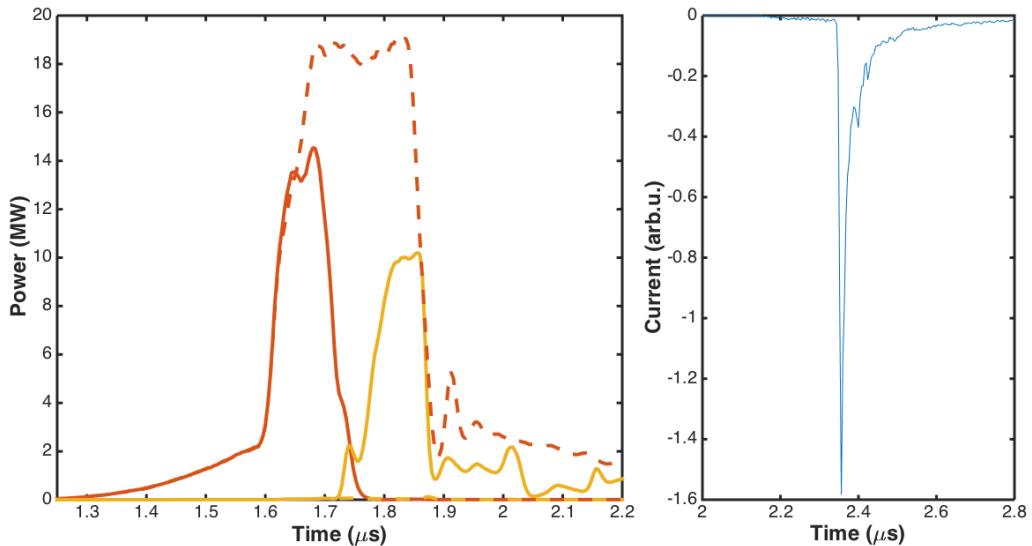


Figure 3.1: RF signals during a breakdown (left) and burst of current emitted, detected by a BPM (right). In the left plot it is clearly visible the fall of the transmitted power (solid red) and the raise of the reflected power (solid yellow). The signals of the previous pulse, so without breakdown, are reported dashed. Note that the time scale in the two plots is not the same. Data acquired with the setup used in this work.

## 3.2 Vacuum arc process description

A fully satisfactory theory to describe the breakdowns has not been formulated yet, but the scientific community produced a number of models to describe the breakdown mechanism and initiation [44]. Most of them converge on the role that the field emission would have in triggering the breakdown, even if inconfutable evidences have to be shown yet.

### 3.2.1 Triggers

The surface of the cathode is not completely flat, but presents some asperities that enhance the field emission as pointed out in chapter 2. This process leads to the formation of hot zones called *field emitters* where the local electric field is enhanced of a factor  $\beta$  because of the geometry and the current emitted is therefore increased (see figure 3.3, box a).

The current flow through the tip heats it up, modifying its physical properties and applying a tensile stress. Theories diverge on the process that takes place at this point: some preprend for the heating up of the tip up to the fusion, like [36]; others on the cracking process of the tip due to the tensile stress applied by the enhanced electric field, which gets comparable to the tensile strength of the material around 10 GV/m [41].

It is in any case possible that during this process the shape of the tip gets modified, enhancing the  $\beta$  factor even more.

### 3.2.2 Plasma initiation

The peculiarity of the breakdown is that is a phenomenon that takes place in vacuum, and has been detected even at large gaps. According to many experimental results, the plasma is created from the cathode material (regardless on how it got emitted from the surface). The cathode material form a neutral gas surrounding the tip, that gets ionised by the electrons emitted by field emission (see figure 3.3, box b). In this first phase the ions created in this manner drift under the effect of the space-charge effect. The plasma initiation last only few ns.

Spectroscopical measurements of the light emitted by the plasma flare have shown that the plasma is formed of ions with various charge and electrons. The DC spark system at CERN showed that the plasma formed by copper cathodes present ionisation levels up to Cu<sup>3+</sup>. [?]

### 3.2.3 Plasma evolution

The ion density of the plasma over the emitter result in the establishment of a sheath potential, which enhances the electrical field, provoking an exponential increase of the field-emitted current. The current emitted reaches values of several A/ $\mu\text{m}^2$ , determining the melting of the emitter (see figure 3.3, box c).

The molten metal becomes part of the plasma, that expands modifying temperature and density. The sheath potential gets modified as well. After an expansion process, where part of the plasma interact with the surface, determining erosion, the greatest part of the ions recombine with the electrons determining an intense optical emission.

### 3.2.4 Cratering phase

During the last plasma expansion, the ions impacting on the surface are expected to create new field emitters. The emitters will melt and result in an explosive emission because of the high field provoked by the sheath potential (see figure 3.3, box d).

The full arc is expected to continue up to the end of the RF pulse. Next the plasma is expected to disappear for expansion cooling or recombination. All the process result in a surface damage in the emitter zone and the surroundings. If in the damaged zone other asperities have been created, them will trigger new breakdowns according to the new value of  $\beta$  (see figure 3.3, box e, f).

In figure 3.2 a photograph of a crater is shown, taken using a scanning emission microscope. Another review about the breakdown mechanism is [37].

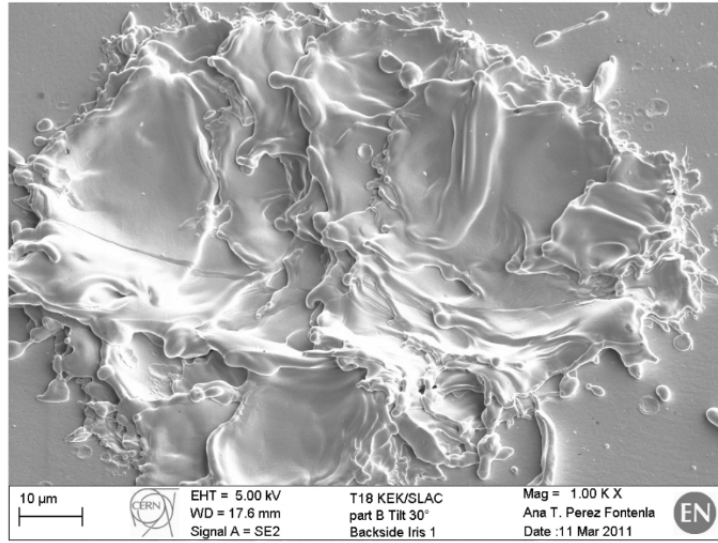


Figure 3.2: Crater provoked by a breakdown in an X-band RF accelerating cavity [30]

## 3.3 Influence of the conditioning process

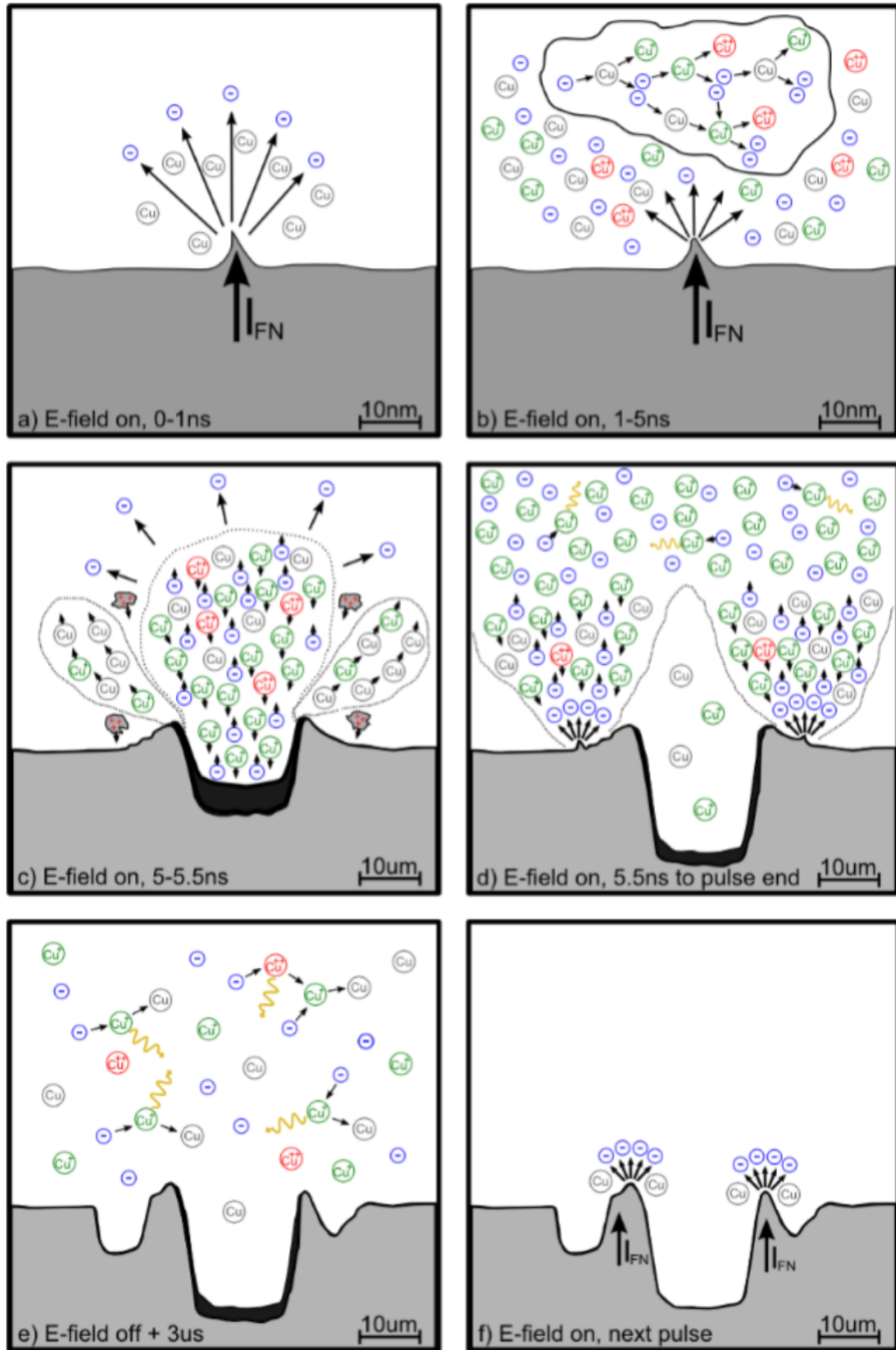


Figure 3.3: Breakdown stages in chronological order. From [25]

# Chapter 4

## Experimental setup

At CERN the high-gradient test are carried on the three X-band test stands (XBOXs), that are setups able to provide the necessary high power RF pulses to the structure under tests. Nevertheless for the tests described in this work the presence of the beam inside the accelerating cavity is necessary, and is provided by the electron linac of the CTF3.

### 4.1 Linac and the Dogleg

#### 4.1.1 The test setup

As mentioned in the first chapter, the main goal of the CTF3 is to demonstrate the feasibility of the CLIC acceleration scheme. For this reason, the linac is used to simulate the Drive Beam to send to the prototypes of Two-beam modules after the recombination process. The linac is realised using the conventional 3 GHz technology, that after the recombination process will lead to the beam frequency of 12 GHz.

Given that the tests of high-gradient cavities is not the design goal of the facility, in the following sections only the relevant part of the setup for the breakdown experiments will be described. The full description of the CTF3 accelerator complex is widely described elsewhere [11, 18, 45].

To realise high-gradient structure tests, a beam line parallel to the linac have been set up. The two beam lines are connected by an oblique segment, giving the characteristic shape that is the origin of the name *Dogleg*.

For the high-gradient testing purpose the accelerator is operated simulating the Main Beam. The parameters of the beam that is possible to produce are reported in the table 4.1

#### Injector

The production of the beam is realised by a 140-kV thermoionic gun, designed to deliver up to 5 A of current in nominal operation conditions. The gun is followed by a S-band prebuncher and a 17 cell travelling-wave buncher. These

---

Current	up to 1.6 A
Pulse length	up to 250 ns
Energy	up to 130 MeV
Repetition freq.	0.83 – 50 Hz

Table 4.1: Beam parameters achievable in the Dogleg [46]

structures are followed by two 1-m long accelerating structures. The beam dimension in this initial phase is controlled using solenoids, that continue up to the second accelerating structure [47].

Downstream the injector a magnetic chicane with collimators is installed to eliminate off-energy particles and to perform the bunch compression [48].

The layout of injector and chicane are reported in figure 4.1.

### Linac

In the linac are installed three modules composed of two S-band accelerating structures operating at 3 GHz. The accelerating structures consist of 32 regular cells, operating in the  $2\pi/3$  mode. The damping of HOMs is guaranteed by the radial slots in the iris containing SiC loads. The structures are designed for the fully loaded operation with a current of more than 4 A, but when simulating the Main Beam the current is significantly less, implying less loading. In this condition the energy gain is essentially bigger compared to when the Drive Beam is simulated.

The focusing is realised by triplets of quadrupoles, coupled with dipole correctors. The beam energy can be measured in the spectrometers in sector 4 and 10.

The layout of the linac is reported in figure 4.2

### The dogleg

After sector 7 in the linac, another triplet of quadrupoles is located on the beamline before a bending magnet. When the bending magnet is on, the beam is directed in the dogleg, passing through an oblique section, to end up in a segment of the beamline parallel to the linac. The optics of the dogleg beamline is designed to correct the dispersion provoked by the bending magnets. At the end of the dogleg line the structure under test is placed between two Beam Position Monitors (BPMs). Just before the structure is placed a slit, in order to protect the coupling cell of the structure from being hit by a misaligned beam. The beam is dumped downstream the structure.

In case the first bending magnet is off, the beam proceeds straight in the linac, passing through a triplet of quadrupoles in section 9 and another triplet in sector 10. After that is placed a spectrometer to measure beam energy and momentum.

The linac proceeds with other accelerating structures, that are not interesting for the development of this work.

## CHAPTER 4. EXPERIMENTAL SETUP

---

The layout of the dogleg and of the linac up to section 10 is reported in figure 4.3.

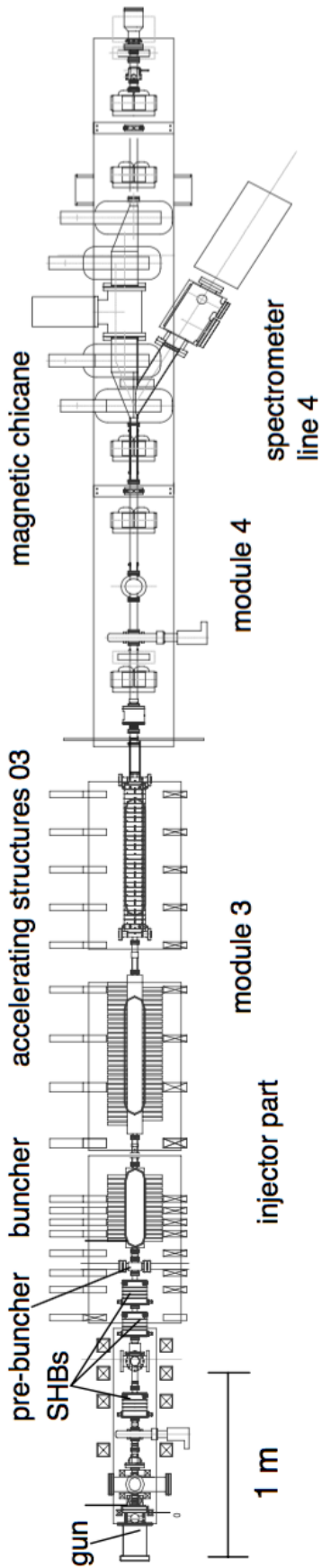


Figure 4.1: Layout of the injector and the magnetic chicane

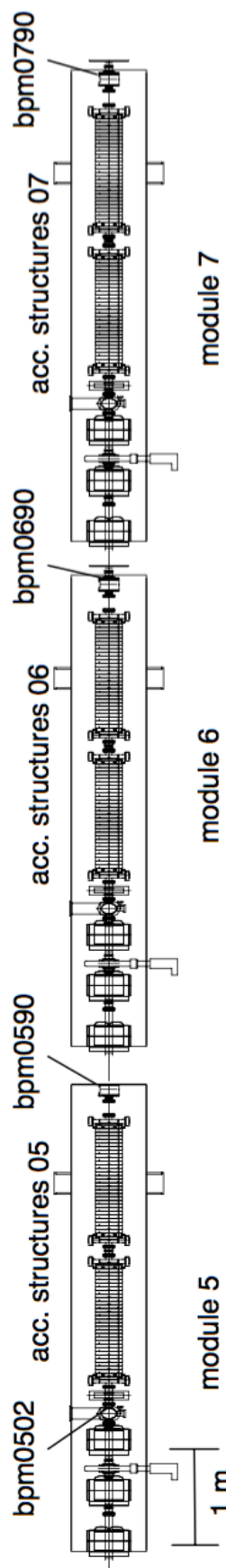


Figure 4.2: Layout of the linac up to module 7

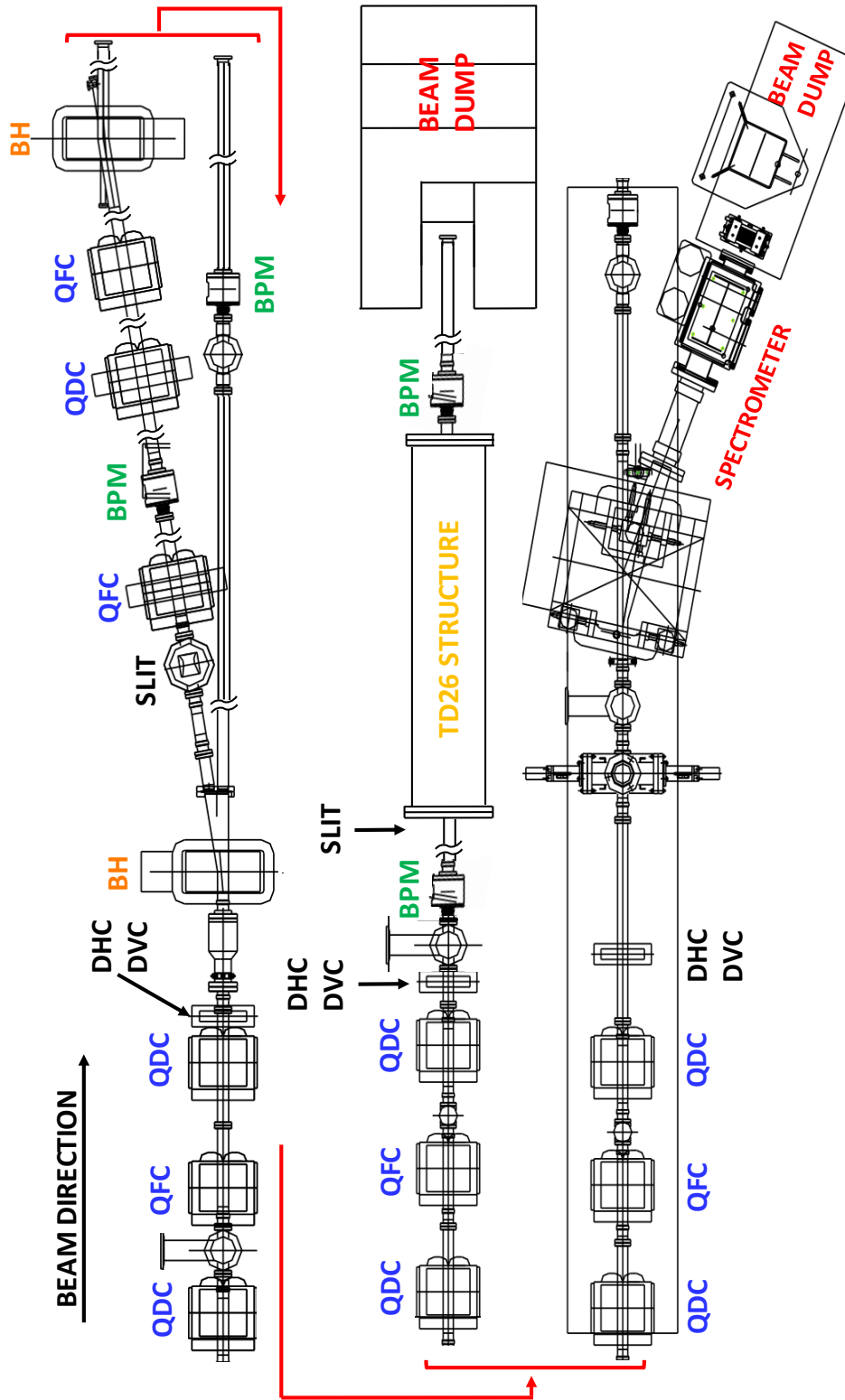


Figure 4.3: Simplified layout of optics and beam instrumentation of the dogleg line, adapted from technical drawings and facility layout [49]. The beam for this section come from the end of the module 7. Legenda: QFC(QDC): focusing(defocusing) quadrupole; DHC(DVC): horizontal(vertical) dipole corrector; BH: bending magnet in horizontal plane; BPM: beam position monitor

### 4.1.2 Comparison of setup and CLIC design

## 4.2 RF power generation

The development of the accelerating cavities technology is strongly related to the possibility to produce and test prototypes. This test activity allows to improve the understanding of the scaling laws of the phenomena that limit the performance of the accelerating structures, but also to compare the results of different production and conditioning techniques.

At CERN the production of 12 GHz RF was carried out just in the CTF3 in the Two-beam modules. These reasons highlighted the necessity of standalone test stands to enlarge the test possibilities. This was realised the first time with the installation of the so called X-Band Test Stand 1 (XBOX1) [50]. Currently there are three X-band test stands active at CERN simultaneously.

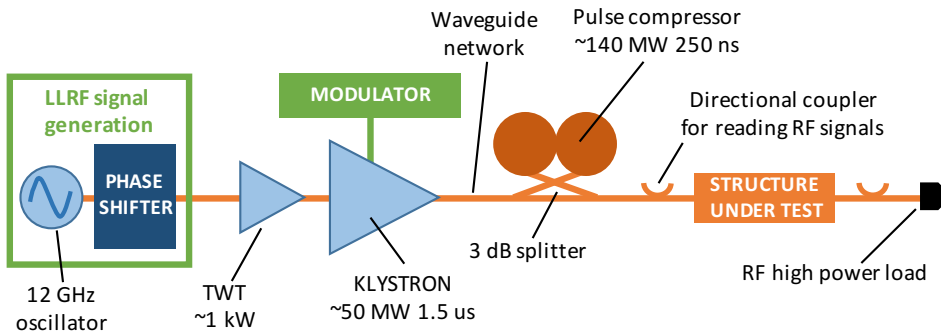


Figure 4.4: Standalone X-band test stand layout. Adapted from [51]

The layout of a RF test stand is shown in figure 4.4. It is normally formed by signal generation, amplification and delivery systems; diagnostic and control systems, and service systems such as cooling and protection systems.

### 4.2.1 The X-Box1 at CERN

The proposal of an X-band test stand at CERN followed the change of the frequency of CLIC from 30 to the european X-band 12 GHz in 2008. An organic description of XBOX1 is in [51, 52]. The high-power RF production is realised using:

- SLAC built XL-5 klystron, able to produce 50 MW of 12 GHz radiation with a pulse length of  $1.5 \mu\text{s}$  and a repetition rate up to 50 Hz.
- Scandinova modulator is used to power the klystron.
- SLED1 type RF pulse compressor is able to compress the klystron output pulse to a shorter one of 140 MW, 250 ns long, which is enough to test accelerating structures considering the waveguide losses.

The RF delivery from the pulse compressor to the structure is realised using WR90 waveguides, kept under high-vacuum at a pressure of the order of  $5 \times 10^{-9}$  mbar. In order to reduce the losses, some part of the line to the structure under test is realised with low loss waveguides. This structure requires mode converters because the fundamental modes of the waveguides are different. The overall transmission of the waveguide from the pulse compressor to the structure under test is around 67 %.

More details regarding the key components of the system are presented in the following sections. The system is controlled solely by the Low-Level Radio Frequency (LLRF), since the gain of the amplification chain is fixed. This feature makes necessary a unique control system of the LLRF together with the Data Acquisition system (DAQ), that will be described in section 4.3.

### **TWT, Klystron and modulator**

The very first power amplification stage is carried out by a NAME OF TWT Travelling Wave Tube (TWT), which is a device with the same working principle of the klystron (described below). It is in charge to raise the power of the signal from some watts to up to 3 kW.

XL-5 klystrons comes from the effort made in SLAC to develop high efficiency klystrons for the Next Linear Collider project (NLC). Them are based on the XL-4 klystrons, adapted from the american X-band frequency of 11.4 GHz to the european 12 GHz. This effort lead to the CPI VKX-8311A tubes that are currently in use[53], which are able to produce a pulse of 50 MW of power,  $1.5 \mu\text{s}$  long with an efficiency of the order of 40%.

Klystrons are vacuum tube amplifiers. Are composed of a thermionic gun, that emits a pulsed beam of electrons. The beam passes through one or several cavities, where a low power RF modulates the beam. After a drift space, where the beam is kept collimated by a solenoid and accelerated by a fixed DC field, the beam passes through a passive cavity that extracts the high power RF. The beam is then dumped.

The klystron is operated in pulsed mode to enhance efficiency. This means that a power supply able to deliver short pulses of high power is necessary. In the XBOX1 is used a K-3 solid state modulator by Sacardinova, able to supply voltage pulses of 410 kV with currents of the order of 310 A.

### **Pulse compressor**

The pulse compressor is the device used to convert the long pulse of the klystron to a shorter one at a higher power. The operation principle is that the power from the klystron is stored in high-Q resonant cavities during the pulse. Before the end of the pulse the cavities are emptied by reverting the phase of the input power. The emptying process is done in a shorter time than the filling one, determining the production of a short high power pulse.

This technique can lead to the peak power increase up to a factor 5-7.

The SLED-I type pulse compressor is using two cavities, coupled with a 3 dB hybrid coupler, in order to discharge the produced power to the desired load instead of sending it back to the klystron. The theory is fully described in [54], the application in XBOX1 in [55].

## 4.3 DAQ & RF control systems

The control system is in charge of generating a phase-modulated signal for the successive amplification stages (TWT and klystron). It also has to acquire the signals from the directional couplers, and the diagnostic signals from the structure and the vacuum systems. According to the diagnostic input, it modulates the signal and can also act on the beam permit of the gun of the linac.

### 4.3.1 Hardware

To perform his task, the control system is made of different components, including PLCs (Programmable Logic Controller) interlock systems, VME (Versa Module Europa) crate based arbitrary signal generators, OASIS PC based digitisers and PXI (PCI eXtension Instrumentation) based control systems.

The core of the system is the National Instrument PXI crate [56], that is the most advanced system in the setup. This carries out: the acquisition and elaboration of all the signals relevant for interlocking the system; trigger the interlocks; save in the internal HDD the recorded signals and retrieve the signals sampled externally in case of an interesting event; interface the rest of the instrumentation.

Since the phase of the LLRF signal has to be modulated to be able to perform the pulse compression, after the generation, the LLRF signal is sent to an analog and a digital phase shifter in series. During the experiments with beam, the digital one is used to phase the beam with the RF feeding the accelerating cavity.

The data acquisition from the -50 dB directional couplers on the waveguides is fulfilled using different kind of sensors:

1. Diodes with a bandwidth of 500MHz convert the RF signals in a DC voltage level
2. IQ demodulators are used to measure the phase and the amplitude
3. Logarithmic detector are used to acquire the signals with a wide dynamic range of over 46 dB

The PXI crate has 8 channels of 14-bits, 250 MSa/s digitisers. These digitisers are connected to an FPGAs to detect if the signals overcome the critical thresholds. In case the FPGA sends a signal to the trigger unit to interlock the LLRF signal production. A 24 channel Digital Multimeter (DMM) unit is used to read the vacuum signals from the ion pump controllers. The fast digitisers acquire the signals from the logarithmic detectors.

The signals of the IQ demodulators are sampled by OASIS acquisition PC containing 16 units of 1 GSa/s, 8-bits ADCs. These are read by the PXI crate and archived only during the breakdown events for the offline analysis.

The signals of the BPMs are acquired and recorded as well by one of the acquisition card of the PXI crate.

### 4.3.2 Online triggers

In order to protect the equipments, a number of parameters are constantly monitored and can interlock the setup. Every piece of the equipment has its internal interlocks defined by the constructor. E.g. in the modulator: pressure in the waveguides, door of the higher radiation zone open, internal arc in the klystron, cooling oil system failure, ...; or in the TWT: reflected power out of scale, ...

The effect of such interlocks is to shut down the affected part, but the rest of the equipment stays on.

A different matter is the interlocking system that is implemented in the PXI crate. When it is triggered, it acts on the LLRF power, cutting the power but leaving the rest of the amplification chain ready. There are four interlocks of this kind, triggered overcoming a user-defined threshold:

1. Peak reflected power:  $\max(P_{REF})$
2. Reflected energy:  $\int P_{REF}(t) dt$
3. Missing transmitted energy:  $\int P_{INC}(t) dt - \int P_{TRA}(t) dt$
4. Peak power reflected to the klystron:  $\max(P_{KREF})$

The last one is again to protect the klystron, and is triggered when the reflected power back from the pulse compressor is too high. This happens especially when the pulse compressor is not properly tuned, as described later in this chapter. The first three indeed are used to detect a breakdown event inside the structure under test. When one or more of these four interlock is triggered, the event is saved by the PXI crate. If no interlock is triggered in one minute, an event is saved as a backup to monitor the state of the current test.

## 4.4 Other systems

mention here thermostatic system of the structure and vacuum system ....

Anything else missing ???

## 4.5 Operation of the setup

- linac switch operation
  - pulse compressor issues
  - relative phase beam / x-band RF

# **Chapter 5**

## **Data analysis tools**

- 5.1 Offline selection of the events**
- 5.2 Time and space positioning of the breakdowns**
- 5.3 Migration of the breakdowns**
- 5.4 Beam induced RF**

# Chapter 6

## Results and future developments

### 6.1 Results

### 6.2 Further developments

### 6.3 Conclusions

During the measurement campaign of this year we learnt how to operate and measure the breakdown rate of the structure with and without beam.

The beam effect analysis has still to be carried on in detail, in particular have to be understood if when running with beam the conditioning takes place or not. Further investigations on this topic require a stable and extensive beam time, which was not the case of the CTF. The comparison of this data with the ones of a stable long test with beam can suggest that switching condition ripetutamente w/ w/o beam can lead to a higher BDR ... - as DC tests suggest - as we cannot see because of the low rep.rate

# List of Abbreviations

BPM	Beam Position Monitor
CDR	Conceptual Design Report
CERN	Conseil européen pour la Recherche nucléaire, Geneva, Switzerland
CLIC	Compact Linear Collider
CTF3	CLIC test facility 3
EEE	Explosive Electron Emission
EFE	Enhanced Field Emission
EM	Electromagnetism -or- electromagnetic
FCC-ee	Future Circular Collider, lepton version
FCC-hh	Future Circular Collider, hadron version
FOM	Figure Of Merit
HOM	High(er) Order Mode
ICFA	International Committee for Future Accelerators
ILC	International Linear Collider
KEK	High Energy Accelerator Research Organization, Tsukuba, Japan
LEP	Large Electron Positron Collider
LHC	Large Hadron Collider
LINAC	Linear Accelerator
LLRF	Low-level RF
NC	Normal Conducting
PETS	Power Extraction and Transfer Structure
RF	Radio frequency
SC	Super Conducting
SLAC	Stanford Linear Accelerator, Menlo Park, California
SM	Standard Model
SPS	Super Proton Synchrotron
SWS	Standing Wave Structure
TBM	Two-Beams module
TDR	Technical Design Report
TE	Transverse Electric (modes of a WG)
TM	Transverse Magnetic (modes of a WG)
TWS	Travelling Wave Structure
TWT	Travelling Wave Tube
WG	Waveguide
XBOX	X-band high power RF test stand

# List of Figures

1.1	Map of the CLIC facility, if implemented in the Geneva area . . . . .	5
1.2	Layout of the final stage of CLIC . . . . .	6
1.3	Design of a Two-beam module. . . . .	7
2.1	Scheme of a travelling wave, disk loaded accelerating structure. The drawings illustrates the input and output couplers, the disks loading the cavity and the beam passing through the irises. From [24] . . . . .	11
2.2	Brillouin diagram of a uniform waveguide (red) compared to a disk-loaded accelerating structure (green) [25] . . . . .	12
2.3	Field enhancement factors for simple geometries of metallic pro- trusions, plotted as function of geometrical features. From [29] .	16
2.4	(a) Electric field distribution around the protrusion considered. (b) Field emitted current and power flow. In both the plots arrows indicate the direction of the field and the color code the absolute value of the field, mapped logarithmically.[36] . . . . .	18
2.5	A disk composing the structure (left) and the scheme of an accelerating structure (right), including couplers for the RF, cooling elements and connection flanges. The wakefield monitor is not present in the prototype under test . . . . .	21
2.6	The structure prototype before the installation ( <i>Photo A. Solodko</i> )	21
3.1	RF signals during a breakdown (left) and burst of current emit- ted, detected by a BPM (right). In the left plot it is clearly visible the fall of the transmitted power (solid red) and the raise of the reflected power (solid yellow). The signals of the previous pulse, so without breakdown, are reported dashed. Note that the time scale in the two plots is not the same. Data acquired with the setup used in this work. . . . .	23
3.2	Crater provoked by a breakdown in an X-band RF accelerating cavity [30] . . . . .	25
3.3	Breakdown stages in chronological order. See text for details. From [25] . . . . .	26
4.1	Layout of the injector and the magnetic chicane . . . . .	30
4.2	Layout of the linac up to module 7 . . . . .	30

## LIST OF FIGURES

---

- |     |  |    |
|-----|--|----|
| 4.3 | Simplified layout of optics and beam instrumentation of the dog-leg line, adapted from technical drawings and facility layout [49]. The beam for this section come from the end of the module 7. Legenda: QFC(QDC): focusing(defocusing) quadrupole; DHC(DVC): horizontal(vertical) dipole corrector; BH: bending magnet in horizontal plane; BPM: beam position monitor . . . . | 31 |
| 4.4 | Standalone X-band test stand layout. Adapted from [51] . . . .   | 32 |

# List of Tables

1.1	Comparison of two circular machines, LEP[7, 8] and FCC-ee[9, 10] and the two projects for linear machines, the fist and last stage of the CLIC implementation [11] and the ILC[12]	4
1.2	CLIC main parameters in the final stage	8
2.1	Parameters of the structure	20
4.1	Beam parameters achievable in the Dogleg [46]	28

# Bibliography

- [1] S. Chatrchyan *et al.*, “Observation of a new boson at a mass of 125 GeV with the CMS experiment at the LHC,” *Phys. Lett.*, vol. B716, pp. 30–61, 2012.
- [2] G. Aad *et al.*, “Observation of a new particle in the search for the Standard Model Higgs boson with the ATLAS detector at the LHC,” *Phys. Lett.*, vol. B716, pp. 1–29, 2012.
- [3] O. S. Bruening, P. Collier, P. Lebrun, S. Myers, R. Ostojaic, J. Poole, and P. Proudlock, *LHC Design Report*. Geneva: CERN, 2004.
- [4] “Icfa statement on linear colliders.” [http://icfa.fnal.gov/statements/icfa\\_lcstatement/](http://icfa.fnal.gov/statements/icfa_lcstatement/). Last accessed: 12 Dec. 2016.
- [5] A. D. Martin, W. J. Stirling, R. S. Thorne, and G. Watt, “Parton distributions for the lhc,” *The European Physical Journal C*, vol. 63, no. 2, pp. 189–285, 2009.
- [6] J. R. Ellis and I. H. Wilson, “New physics with the compact linear colider,” *Nature*, vol. 409, pp. 431–435, 2001.
- [7] S. Aull, M. Benedikt, D. Bozzini, O. Brunner, J.-P. Burnet, A. Butterworth, R. Calaga, E. Jensen, V. Mertens, A. Milanese, M. Nonis, K. Oide, N. Schwerg, L. Tavian, J. Wenninger, F. Zimmermann, L. Rinolfi, A. Blondel, M. Koratzinos, and S. Gorgi Zadeh, “Electrical Power Budget for FCC-ee,” May 2016.
- [8] P. Brown, O. C. Brunner, A. Butterworth, E. Ciapala, H. Frischholz, G. Geschonke, E. Peschardt, and J. P. H. Sladen, “Ultimate Performance of the LEP RF System,” p. 5 p, Jun 2001.
- [9] J. Wenninger *et al.*, “Future Circular Collider Study - Lepton Collider Parameters,” Tech. Rep. FCC-1401201640-DSC, CERN, Geneva, Jun 2016.
- [10] F. Zimmermann, M. Benedikt, K. Oide, A. Bogomyagkov, E. Levichev, M. Migliorati, and U. Wienands, “Status and Challenges for FCC-ee,” Tech. Rep. CERN-ACC-2015-0111, CERN, Geneva, Aug 2015.

## BIBLIOGRAPHY

---

- [11] M. Aicheler, P. Burrows, M. Draper, T. Garvey, P. Lebrun, K. Peach, N. Phinney, H. Schmickler, D. Schulte, and N. Toge, “A Multi-TeV Linear Collider Based on CLIC Technology: CLIC Conceptual Design Report,” Tech. Rep. CERN-2012-007. SLAC-R-985. KEK-Report-2012-1. JAI-2012-001, Geneva, 2012.
- [12] T. Behnke, J. E. Brau, B. Foster, J. Fuster, M. Harrison, J. M. Patterson, M. Peskin, M. Stanitzki, N. Walker, and H. Yamamoto, “The International Linear Collider - Volume 1: Executive Summary,” Tech. Rep. CERN-ATS-2013-037. ILC-REPORT-2013-040. KEK-Report-2013-1., Geneva, Jun 2013.
- [13] P. Lebrun, L. Linssen, A. Lucaci-Timoce, D. Schulte, F. Simon, S. Staines, N. Toge, H. Weerts, and J. Wells, “The CLIC Programme: Towards a Staged  $e^+e^-$  Linear Collider Exploring the Terascale: CLIC Conceptual Design Report,” Tech. Rep. CERN-2012-005, Geneva, 2012.
- [14] M. J. Boland, U. Felzmann, P. J. Giansiracusa, T. G. Lucas, R. P. Rassool, C. Balazs, T. K. Charles, K. Afanaciev, I. Emeliantchik, and Ignatenko, “Updated baseline for a staged Compact Linear Collider,” Tech. Rep. CERN-2016-004, Geneva, Aug 2016.
- [15] I. Bozovic-Jelisavcic, “CLIC Physics Overview,” Tech. Rep. CLICdp-Conf-2016-006, CERN, Geneva, Jun 2016.
- [16] P. G. Roloff, “Higgs Physics at the CLIC Electron-Positron Linear Collider,” Tech. Rep. CLICdp-Pub-2016-001, CERN, Geneva, Aug 2016.
- [17] R. Corsini, “First Full Beam Loading Operation with the CTF3 Linac,” Aug 2004.
- [18] R. Corsini, “Experimental verification of the CLIC two-beam scheme, status and outlook,” *Conf. Proc.*, vol. C1205201, p. TUOBC01. 3 p, May 2012.
- [19] M. Weiss, “Introduction to rf linear accelerators,” *CAS - CERN Accelerator school: 5th General accelerator physics course*, 1994.
- [20] T. P. Wangler, *RF linear accelerators; 2nd rev. version*. Weinheim: Wiley-VCH, 2008.
- [21] S. Humphries, *Principles of charged particle acceleration*. New York, NY: Wiley, 1986.
- [22] E. Botta and T. Bressani, *Elementi di elettromagnetismo avanzato*. Aracne editrice, 1 ed., Jan 2009.
- [23] J. D. Jackson, *Classical electrodynamics; 2nd ed.* New York: Wiley, 1975.

## BIBLIOGRAPHY

---

- [24] A. Streun, “Experimental methods of particle physics - particle accelerators. lecture slides.” <https://ados.web.psi.ch/empp-streun/empp.pdf>. Last accessed 4 Feb 2017.
- [25] J. W. Kovermann, A. Stahl, and W. Wuensch, *Comparative Studies of High-Gradient Rf and Dc Breakdowns*. PhD thesis, Aachen, Tech. Hochsch., Aachen, 2010. Presented 17 Dec 2010.
- [26] F. Tecker, “RF Systems,” *CAS - CERN Accelerator school: Introduction to Accelerator Physics 2016*, Oct 2016.
- [27] J. W. Wang and G. A. Loew, “Field emission and RF breakdown in high gradient room temperature linac structures,” in *Frontiers of accelerator technology. Proceedings, Joint US-CERN-Japan International School, Hayama and Tsukuba, Japan, September 9-18, 1996*, pp. 768–794, 1997.
- [28] R. H. Fowler and L. Nordheim, “Electron emission in intense electric fields,” *Proceedings of the Royal Society of London A: Mathematical, Physical and Engineering Sciences*, vol. 119, no. 781, pp. 173–181, 1928.
- [29] F. Rohrbach, *Sur les mécanismes qui conduisent à la formation de l'étincelle électrique à très haute tension et sous ultra-vide par la mesure des temps de retard à la disruption*. Geneva: CERN, 1971.
- [30] W. Wuensch, “Advances in the Understanding of the Physical Processes of Vacuum Breakdown,” Tech. Rep. CERN-OPEN-2014-028. CLIC-Note-1025, CERN, Geneva, May 2013.
- [31] W. D. Kilpatrick, “Criterion for vacuum sparking designed to include both rf and dc,” *Review of Scientific Instruments*, vol. 28, no. 10, pp. 824–826, 1957.
- [32] J. W. Wang, “Some problems on RF breakdown in room temperature accelerator structure: a possible criterion,” Tech. Rep. SLAC/AP-051, 1986.
- [33] A. S. Verdu, “Kilpatrick’s critereon, an historical perspective.” [http://indico.cern.ch/event/76081/contributions/2086273/attachments/1051717/1499553/Kilpatricks\\_Criterion.pdf](http://indico.cern.ch/event/76081/contributions/2086273/attachments/1051717/1499553/Kilpatricks_Criterion.pdf), December 2009. Last accessed: 31 Jan 2017.
- [34] W. Wuensch, “The Scaling of the Traveling-Wave RF Breakdown Limit,” Tech. Rep. CERN-AB-2006-013. CLIC-Note-649, CERN, Geneva, Jan 2006.
- [35] W. Wuensch, “Observations about RF Breakdown from the CLIC High Gradient Testing Program,” Dec 2006. revised version submitted on 2006-12-12 10:52:40.

## BIBLIOGRAPHY

---

- [36] A. Grudiev, S. Calatroni, and W. Wuensch, “New local field quantity describing the high gradient limit of accelerating structures,” *Phys. Rev. Spec. Top. Accel. Beams*, vol. 12, p. 102001, 2009.
- [37] E. A. Litvinov, G. A. Mesyats, and D. I. ProskurovskiÄ, “Field emission and explosive electron emission processes in vacuum discharges,” *Soviet Physics Uspekhi*, vol. 26, no. 2, p. 138, 1983.
- [38] A. Grudiev and W. Wuensch, “Design of the Clic main Linac accelerating structure for Clic conceptual design report,” p. 3 p, Sep 2010.
- [39] A. Lunin, V. Yakovlev, and A. Grudiev, “Analytical solutions for transient and steady state beam loading in arbitrary traveling wave accelerating structures,” *Phys. Rev. Spec. Top. Accel. Beams*, vol. 14, p. 052001. 11 p, Dec 2010.
- [40] D. Alpert, D. A. Lee, E. M. Lyman, and H. E. Tomaschke, “Initiation of electrical breakdown in ultrahigh vacuum,” *Journal of Vacuum Science and Technology*, vol. 1, no. 2, pp. 35–50, 1964.
- [41] Z. Insepov, J. Norem, S. Veitzer, and S. Mahalingam, “Modeling Arcs,” Tech. Rep. arXiv:1108.0861, Aug 2011. Comments: 6 pages, 5 figures.
- [42] W. Wuensch, “High Gradient Breakdown in Normal-Conducting RF Cavities,” 2002.
- [43] R. Rajamaki, W. Wuensch, and V. Koivunen, *Vacuum arc localization in CLIC prototype radio frequency accelerating structures*. PhD thesis, Aalto U., Otaniemi, Espoo (Finland), Apr 2016. Presented 19 Jan 2016.
- [44] D. K. Davies, “The initiation of electrical breakdown in vacuum. a review,” *Journal of Vacuum Science and Technology*, vol. 10, no. 1, pp. 115–121, 1973.
- [45] R. D. Ruth, “CTF3 Design Report,” Tech. Rep. SLAC-PUB-9672, Stanford, CA, 2003. Submitted on 13 Mar 2003.
- [46] J. L. Navarro Quirante, R. Corsini, A. Degiovanni, S. Döbert, A. Grudiev, O. Kononenko, G. McMonagle, S. Rey, A. Solodko, I. Syratchev, F. Tecker, L. Timeo, B. Woolley, X. Wu, W. Wuensch, O. Kononenko, A. Solodko, J. Tagg, B. Woolley, and X. Wu, “Effect of Beam-Loading on the Breakdown Rate of High Gradient Accelerating Structures,” p. TUPP033. 3 p, 2014.
- [47] A. D. Yeremian, R. Miller, R. D. Ruth, H. H. Braun, G. Geschonke, L. Groening, L. Rinolfi, L. Thorndahl, I. H. Wilson, and F. Zhou, “CTF3 drive-beam injector design,” Sep 2002.

## BIBLIOGRAPHY

---

- [48] H. H. Braun, R. Corsini, S. Döbert, E. Jensen, F. A. Tecker, and P. Urschütz, “Efficient long-pulse fully-loaded CTF3 linac operation,” Tech. Rep. CERN-OPEN-2006-070. CLIC-Note-697, CERN, Geneva, Nov 2006.
- [49] “Ctf3 design and layout.” <https://edms.cern.ch/ui/#!master/navigator/project?P:1972521142:1236731031:subDocs>. Last accessed: 7 Feb 2017.
- [50] F. Peauger, A. Hamdi, S. Curt, S. Doeberl, G. McMonagle, G. Rossat, K. Schirm, I. Syratchev, L. Timeo, S. Kuzikov, A. Vikharev, A. Haase, D. Sprehn, A. Jensen, E. Jongewaard, C. Nantista, and A. Vlieks, “A 12 GHZ RF Power source for the CLIC study,” p. 4 p, May 2010.
- [51] B. J. Woolley, *High power X-band RF test stand development and high power testing of the CLIC crab cavity*. PhD thesis, Lancaster U., Aug 2015.
- [52] J. Kovermann, N. Catalan-Lasheras, S. Curt, S. Doeberl, M. Naon, G. McMonagle, E. Paju, S. Rey, G. Riddone, K. Schirm, I. Syratchev, L. Timeo, W. Wuensch, A. Hamdi, F. Peauger, J. Eichner, A. Haase, and D. Sprehn, “Commissioning of the First Klystron-Based X-Band Power Source at CERN,” *Conf. Proc.*, vol. C1205201, p. THPPC060. 3 p, May 2012.
- [53] “Cpi x-band klystron vkx-8311a specifications.” <http://www.cpii.com/docs/datasheets/154/VKX-8311A%20Datasheet.pdf>. Last accessed: 22 Feb 2017.
- [54] A. Fiebig and C. Schieblich, “A SLED type pulse compressor with rectangular pulse shape,” p. 4 p, Jun 1990.
- [55] A. Bogdashov, G. Denisov, S. Kuzikov, A. Vikharev, K. Schirm, and I. Syratchev, “A 12 GHz pulse compressor and components for the CLIC test stand,” *Proc. RuPAC-2010, Protvino, Russia*, p. TUPSA005. 4 p, 2010.
- [56] “National instrument pxi systems.” <http://www.ni.com/pxi/>. Last accessed: 21 Feb 2017.